The Classification Between Prostate Transitional Zone Cancer and Hyperplasia Using Deep Transfer Learning from Disease-Related Images: A Retrospective Study

Bo Hu
Fourth Military Medical University
Lin-Feng Yan
Fourth Military Medical University
Yang Yang
Fourth Military Medical University
Ying-Zhi Sun
Fourth Military Medical University
Cui Yue
Fourth Military Medical University
Dong Wu
Fourth Military Medical University
Wen Wang (wangwen@fmmu.edu.cn)
Tangdu Hospital, Fourth Military Medical Univwersity https://orcid.org/0000-0001-6473-4888
Di Zhao
Computer Network Information Center Chinese Academy of Sciences
Guang-Bin Cui
Fourth Military Medical University

Research article

Keywords: deep learning, transfer learning, magnetic resonance imaging (MRI), prostate cancer

Posted Date: July 20th, 2020

DOI: https://doi.org/10.21203/rs.3.rs-41679/v1

Abstract

Background The diagnosis of prostate transition zone cancers (PTZC) remains a clinical challenge due to its similarity to benign prostatic hyperplasia (BPH) on MRI. The Deep Convolutional Neural Networks showed high efficacy in medical imaging but was limited by the small data size. A transfer learning method was combined with deep learning to overcome this challenge.

Methods A retrospective investigation was conducted on 217 patients enrolled from our hospital database (208 patients) and The Cancer Imaging Archive (9 patients). Based on the T2 weighted images (T2WIs) and apparent diffusion coefficient (ADC) maps of these patients, DCNN models were trained and compared between different TL database (ImageNet vs. disease-related images) and protocols (from scratch, fine-tuning or transductive transferring).

Results PTZC and BPH can be classified through traditional DCNN. The efficacy of transfer learning from ImageNet was limited but improved by transferring knowledge from the disease-related images. Furthermore, transductive transfer learning from disease-related images had the comparable efficacies with the fine-tuning method. Limitations include retrospective design and relatively small sample size.

Conclusion For PTZC with a small sample size, the accurate diagnosis can be achieved via the deep transfer learning from disease-related images.

1. Background

About 25% prostate cancers originate in transition zone (TZ), and its diagnosis remains a clinical challenge, due to its similarity to benign prostatic hyperplasia (BPH) on MRI [1, 2]. The conventional transrectal ultrasound-guided biopsy face the dilemma of both underdiagnoses and overdiagnosis because of its invasive nature, the small size of minute tumor, and instinct limitations of H&E slides [3, 4]. In addition, the screening efficacy in developing areas are impaired by the lack of radiology interpretation expertise. Consequently, several machine learning methods were investigated to classify prostate cancer from normal tissue or BPH [5, 6].

Traditional machine learning methods are laborious because of the complex feature extraction procedure [7, 8]. Most importantly, the selection of feature may be influenced by different data sources and processing software, thus its generalization is limited. The Deep Convolutional Neural Networks (DCNN) automatically extract features in medical imaging diagnosis based on fixed architectures [9–11]. Besides, several deep learning studies were based on multi-center database, which proved the robustness of DCNN model [12, 13]. However, the DCNN model is a data-dependent classifier, in which a larger database yields a better result, but prostate TZ cancer (PTZC) images are usually scarce [2]. DCNN is developed to imitates how the visual cortex of the brain processes and recognizes images, but the learning procedure has always been regarded as a “black box” [14]. Human can learn one thing much easier and faster if they had learnt similar things at before, which is called transfer learning (TL). In machine learning, TL is designed to transfer the information from a certain source domain to the target domain [15, 16]. This

method is usually combined with deep learning to overcome the issue of small sample size [17, 18]. By transferring similar features from everyday pictures to disease, previous DCNN studies proved the efficacy of TL based on a big natural image database called ImageNet [12, 19, 20].

However, a more effective way for human to learn one disease is to analogically learn another similar disease. The imaging manifestation of PTZC is similar to prostate peripheral zone cancer (PPZC) in some ways, and the data of PPZC is far more fruitful [21]. Consequently, to deal with the scarcity of PTZC and better differentiate it from BPH, we decided to imitate the analogical learning ability of human brain by combining TL and DCNN. In this current study, we trained DCNN models and compared varied TL database [ImageNet (natural images) vs. PPZC images (disease-related images)] and protocols (from scratch, fine-tuning or transductive transferring).

2. Methods

2.1. Patients

From May 2010 to March 2016, the detailed clinical information and MRI images of 309 patients from our Hospital were retrospectively recruited. After excluding patients received previous surgery or medication, lacked pathological diagnosis or with poor MRI qualities, 208 pathologically confirmed prostate cancer or BPH patients were enrolled in the current study. These patients underwent a series of MR scanning followed by radical prostatectomy or MRI-guided biopsy within a month. Gleason score equal or higher than 6 was considered as malignant tumor. Imaging data of these 208 patients from local dataset were enrolled, and their basic information was showed in Table 1. In addition, 9 PTZC patients from The Cancer Imaging Archive (TCIA)[22] were enrolled and resulted in a final enrollment of 217 patients. Among these 217 patients, 81 were PPZC patients, 30 were PTZC patients and 106 were BPH patients (Fig. 1).

Table 1
The basic information (standard deviation) of patients of the local dataset.

Clinical features	PCA	BPH	P value
Age	70.44 (± 9.73)	70.07 (± 7.94)	0.73
Weight (kg)	67.72(± 10.60)	67.58(± 10.86)	0.92
Blood Glucose (((mm/L	5.68(± 0.95)	5.65(± 1.78)	0.84
F-PSA (ng/ml)	24.00(42.93)	3.50(5.50)	< 0.001
T-PSA (ng/ml)	387.58(837.62)	21.06(45.00)	< 0.001
F/T	0.12(0.44)	0.18(0.08)	< 0.001

2.2. Imaging data

MRI protocols were implemented on three 3T (GE DISCOVERY MR750, GE SIGNA EXCITE and MAGNETOM Skyra) and two 1.5T scanners (GE SIGNA HDxt and SIEMENS Area). All parameters of local scanner were provided in **Table S1**. Patients had received axial T2 weighted images (T2WIs) and axial multiple b value DWI (multi-b DWI) scans. Apparent diffusion coefficient (ADC) maps were calculated by using two different b values (0 and 1,000 s/mm^2). Images from TCIA included axial T2WIs and axial ADC maps.

2.3. Preprocessing

Images were converted from DICOM to bitmap format. The locations of individual lesions on the MR image were independently determined by 2 radiologists with 15 years' experience (C.Y. and YZ.S.) (Fig. 2). After these 2 experienced radiologists read both modalities of images of 1 patient, ROIs were drawn by hand on all modalities and planes that the tumor is visible. If their decision are inconsistent, a senior radiologist with more than 20 years experience would make the final decision (GB.C.) After that, the target lesion was cropped with a rectangular ROI, in which the tumor locates in the center of the image and occupies about 80% area. These cropped images were then resized to a 256 × 256 matrix by using bilinear interpolation method.

Data augmentation plays a vital role in the utilization of DCNN, and it can significantly improve the efficacy of DCNN classifier [23]. Images were augmented by using random cropping, mean subtraction, and mirror images, which were prebuilt options within the Caffe framework. Further augmentation includes 90°-rotation, vertical flipping, adding standard gaussian white noise and histogram equalization processed by using MATLAB (Matrix Laboratory 2016b, Mathworks, Natick, MA)[24]. Since some of these processed images are intrinsically different to the original images, test sets were not augmented all through the project to prevent biases.

2.4. Training procedure

Prostate images were processed via a series of operations to produce a predicting probability for each image. DCNN include diverse layers to form a pipeline of imaging features extraction and export final output of these labels (i.e. The possibility of malignancy and hyperplasia for each cropped image.). These procedures were conducted with the "weights" in the whole network, which were randomly initialized before the training procedure. A DCNN is trained to discover and optimize the "weights". After dozens or hundreds of training, an optimized set of "weights" could be obtained to exert a satisfying predicting ability [18].

2.5. Transfer learning procedure

TL can improve a classifier in one domain by transferring knowledge from a larger relevant domain. In some cases, this goal can be achieved by using the “off-the-shelf” “weights” trained with data from the relevant domain (Fig. 3c**)**. The transferred “weights” could be used directly to classify the target data, a process often called transductive TL [16]. In other cases, the “weights” of the network are retrained with the target data, a process often called “fine-tuning”(Fig. 3b**)**[17]. These 2 methods were both testified in the current study.

2.6. Statistical analysis

For each image, the probability to be a malignant lesion was defined to be the final output. On the test datasets, receiver operating characteristic (ROC) curves were plotted according to these output values, and area under the curves (AUCs) and their 95% confidence intervals (CI) were determined [25]. For these ROC curves, comparisons between AUCs were made with DeLong and Clarke-Pearson method[26], and *P* values less than 0.05 were considered as statistically significant. When it came to multiple comparison tests, *P* values were corrected through a *post hoc* Bonferroni method[27]. The optimal accuracy, sensitivity, and specificity were determined from the optimal cutoff value by the Youden Index (YI) according to the following equation: YI = [1 - (sensitivity + sensitivity)]. Statistics analysis and graph plotting were implemented in Sigmaplot 12.5 software (Systat Software, Inc, Point Richmond, CA).

3. Result

3.1. PTZC and BPH could be classified with Alex-Net DCNN

Of the 106 BPH patients, 30 BPH patients were randomly selected as the counterpart of the 30 PTZC patients. Images of the 60 selected patients were defined as our target dataset to train and test an Alex-Net DCNN. The 60 patients in target dataset were randomly divided into a test set (20 patients, 110 pictures) and a training set (40 patients, 2320 pictures after data augmentation) **(**Fig. 4a**-iii)**. Then, 5 Alex-net models were trained through a 5-fold cross-validation method. In each training procedure, 4/5 data in training set was used to train the model, while the rest 1/5 was used as the validation set to select the optimal model. After that, the test set was used to testify the efficacy of those 5 models, and for each image, 5 probabilities (to be malignant) were derived. In the end, 5 probabilities of each image were averaged to calculate the final output value.

Even with the small sample size, PTZC and BPH can be distinguished using DCNN model **(**Fig. 4b, Without TL modal**)**. Using only PTZC and BPH data, T2WIs were associated with the AUC of 0.73 (95% CI = 0.63–0.83), as well as the sensitivity, specificity and accuracy of 69%, 75% and 81%, respectively. ADC images were associated with the AUC of 0.94 (95% CI = 0.90–0.99), as well as the sensitivity, specificity and accuracy of 84%, 97% and 89%, respectively. The diagnostic efficacy of Alex-Net DCNN model using ADC images was quite satisfying, but that using T2WI needed to be improved further.

3.2. The performance of TL from natural pictures (ImageNet) is limited by small data size

An Alex-Net DCNN model were pre-trained with 1.2 million natural color pictures of ImageNet **(**Fig. 4a**-ii)** [28], and then, it was fine-tuned by using aformentioned target data (60 PTZC and 60 BPH patients).

Using pre-trained model with ImageNet (Fig. 4b, TL-ImageNet), T2WIs were associated with the AUC of 0.75 (95% CI = 0.65–0.84), as well as the sensitivity, specificity, and accuracy of 76%, 73% and 75%, respectively. ADC images were associated with the AUC of 0.96 (95% CI = 0.90–0.99), as well as the sensitivity, specificity, and accuracy of 84%, 97% and 89%, respectively. TL from ImageNet resulted in slight improvement of efficacies based on T2WIs (P = 0.17) and ADC images (P = 0.07) than those without TL.

3.3. TL from disease-related images (PTZC images) improved the diagnostic efficacy of DCNN model

Another TL model was pre-trained with images of the rest 76 BPH and 81 PTZC patients **(**Fig. 4a-i**)**. This pre-trained model was fine-tuned with the aforementioned target dataset (60 PTZC and 60BPH patients).

Using the model trained from the disease-related dataset (Fig. 4b, TL-Related dataset), T2WIs were associated with the AUC of 0.86 (95% CI = 0.79–0.93), as well as the sensitivity, specificity, and accuracy of 90%, 69% and 80%, respectively. The diagnostic efficacy of TL-Related dataset model was significantly higher than that of Without TL model (P = 0.00014) or TL-ImageNet model (P = 0.00046).

ADC images were associated with the AUC of 0.97 (95% CI = 0.90–0.99), as well as the sensitivity, specificity, and accuracy 90%, 94% and 92%, respectively. However, there was no significant difference between AUCs of TL-Related dataset model and TL-ImageNet model (P = 0.88), or between TL-Related dataset model and Without TL model (P = 0.29).

3.4. Transductive method is a novel and effective way for TL

A transductive Google-Net and a transductive Alex-Net models were separately trained with the TL-Related dataset (images of 81 PPZC and 76 BPH patients), and the models were directly used to classify all PTZC and BPH images (Fig. 3c). Finally, ROC curves and the AUCs were obtained (Fig. 5).

Using the transductive Google-Net model, T2WIs were associated with the AUC of 0.86 (95% CI = 0.83–0.89), as well as the sensitivity, specificity, and accuracy of 84%, 73% and 79%, respectively. ADC images were associated with the AUC of 0.98 (95% CI = 0.97–0.99), as well as the sensitivity, specificity, and accuracy of 94%, 92% and 93%, respectively.

Using the transductive Alex-Net model, T2WIs were associated with the AUC of 0.89 (95% CI = 0.86–0.91), as well as the sensitivity, specificity, and accuracy of 81%, 82% and 81%, respectively. ADC images were associated with the AUC of 0.98 (95% CI = 0.97–0.99), as well as the sensitivity, specificity, and accuracy of 97%, 93% and 95%, respectively.

3.5. Ensemble contributes to the stabilization of output values

Because each lesion may have multiple planes, ensembles were performed by averaging the output values of these planes to get a stable predicting output. Of these 20 patients, 2 patients were misdiagnosed with images of T2WI, while in ADC images, only 1 patient was misdiagnosed (Fig. 6).

4. Discussion

Based on the current investigations, we revealed that PTZC and BPH can be distinguished through traditional DCNN. The efficacy of TL from ImageNet to T2WI and ADC images was limited but that from the disease-related images significantly improved the diagnostic efficacy of T2WI. Besides, transductive TL from disease-related images had similar diagnostic efficacies to fine-tuning method on both T2WI and ADC images. In addition, we found that DCNN model is robust enough to process images from different source.

The efficacy of TL from ImageNet was proved to be significant in previous studies, but their findings contradicted with ours [12, 18, 29]. In our study, the diagnostic efficacy was improved by TL from natural images, but the improvement was not significant. This maybe because of that the DCNN model had indeed learned useful texture characteristics from natural images and had applied it on the diagnosis of prostate TZ cancer, but the efficacy was still limited with the small sample size of rare disease. On the contrary, the DCNN model trained with disease-related images performed significantly, which means the DCNN model is to some extent like human brain network, and learning directly from related disease is definitely a more effective way. There were also studies that focused on transductive TL, but according to our knowledge, very few studies had applied this method on medical images[30–32]. It is worth testing the application possibility of transductive DCNN for diseases before it can step from bench to bed. In the future, this TL method could be used to diagnose rare diseases, such as differentiating lung cancer cell lymphatic metastasis from normal lymphatic tissue by transferring information from lung cancer.

Previous researches suggests that the DCNN is effective in classifying prostate cancer and BPH or other benign lesions, but few researches were specifically conducted to classify PTZC and BPH [33–35]. This issue should be concerned, because the diagnostic accuracy between PTZC and BPH in previous studies may be biased with the far more PPZC patients. These studies also revealed that T2WI and ADC map are two most efficient protocols. We revealed that the diagnostic efficacy of T2WI was lower than ADC images when the sample size is small, which was partly made up by TL. As a result, we assumed that

although imaging features of ADC images were simple and effective, the potential of T2WI could be tapped more fully by experienced radiologists. In the developing regions where the advanced MRI is lacked, the full utilization of T2WIs using the current TL-DCNN strategy could be a critical and practical way to improve the diagnostic efficacy.

Our study has two limitations. First, although we applied a TL method to make up for the shortcomings caused by the small sample size, it still had limited help for practical applications. Second, because of the retrospective nature of the current study, some bias cannot be ruled out, thus a randomized controlled trials (RCT) should be conducted in the future.

5. Conclusion

The diagnostic efficacy of the Alex-Net model for differentiating PTZC and BPH could be significantly improved by transferring the disparity information between PPZC and BPH, which was obviously better than TL from ImageNet. Furthermore, transductive TL model trained with the data of PPZC and BPH could be directly used to classify PTZC from BPH.

Abbreviations

PPZC: prostate peripheral zone cancer; PTZC: prostate transitional zone cancer; BPH: benign prostatic hyperplasia; DCNN: deep convolutional neural network; ROI: region of interest; ROC: receiver operating characteristic; AUC: area under the curve; MRI: magnetic resonance imaging.

Declarations

Ethics approval and consent to participate

All experiments conformed to the principles of the Declaration of Helsinki and was approved by the ethics committee of Tangdu Hospital of Fourth Military Medical University. All participants provided informed written consent.

Consent for publication

Written informed consent for publication was obtained from all participants.

Availability of data and material

Please contact authors for data requests.

Competing interest

The authors declare no potential conflicts of interest.

Funding

This paper was sponsored by the National Key Research and Development Program of China (Collection of the data; No. 2016YFC0107105, to Dr. Cui GB), the Innovation Foundation of Tangdu Hospital (Analysis of the data; No. 2016LCYJ001, to Dr. Cui GB) and Young Talent Grant of the University (Analysis of the data; to Dr. Wang W).

Authors' contributions

All authors have read and approved the manuscript. WW and GBC, Conceptualization; DW, Data curation; LFY, Formal analysis; WW and GBC, Funding acquisition; BH, Investigation; DZ, Methodology; YZS and CY, Resources; WW and GBC, Supervision; YY, Validation; BH, Visualization; BH, Roles/Writing - original draft; WW, Writing - review & editing

Acknowledgement

We would like to thank Dr. Cui Wu-Xun and Mrs. Xiu Si-Jie for the excellent work in helping collect the MRI images. We would like to thank Pathology Department of Tangdu hospital for their supports. The authors thank Mr. Xiao-Cheng Wei (MR research, GE Healthcare China) for the excellent support.

References

1. Hoeks CM, Hambrock T, Yakar D, Hulsbergen-van de Kaa CA, Feuth T, Witjes JA, Futterer JJ, Barentsz JO: **Transition zone prostate cancer: detection and localization with 3-T multiparametric MR imaging**. *Radiology* 2013, **266**(1):207-217.
2. Patel V, Merrick GS, Allen ZA, Andreini H, Taubenslag W, Singh S, Butler WM, Adamovich E, Bittner N: **The incidence of transition zone prostate cancer diagnosed by transperineal template-guided mapping biopsy: implications for treatment planning**. *Urology* 2011, **77**(5):1148-1152.
3. Loeb S, Bjurlin MA, Nicholson J, Tammela TL, Penson DF, Carter HB, Carroll P, Etzioni R: **Overdiagnosis and overtreatment of prostate cancer**. *European urology* 2014, **65**(6):1046-1055.
4. Bonkhoff H: **Significance of prostate cancer missed on needle biopsy tools for retrieving missed cancer**. *The Prostate* 2016, **76**(4):369-375.
5. Iyama Y, Nakaura T, Katahira K, Iyama A, Nagayama Y, Oda S, Utsunomiya D, Yamashita Y: **Development and validation of a logistic regression model to distinguish transition zone cancers from benign prostatic hyperplasia on multi-parametric prostate MRI**. *European radiology* 2017, **27**(9):3600-3608.

6. Kuess P, Andrzejewski P, Nilsson D, Georg P, Knoth J, Susani M, Trygg J, Helbich TH, Polanec SH, Georg D *et al*: **Association between pathology and texture features of multi parametric MRI of the prostate**. *Physics in medicine and biology* 2017, **62**(19):7833-7854.
7. Adankon MM, Cheriet M: **Support Vector Machine**. *Computer Science* 2002, **1**(4):1-28.
8. Hosmer DW, Hosmer T, Le CS, Lemeshow S: **A comparison of goodness-of-fit tests for the logistic regression model**. *Statistics in Medicine* 2015, **16**(9):965-980.
9. Szegedy C, Liu W, Jia Y, Sermanet P, Reed S, Anguelov D, Erhan D, Vanhoucke V, Rabinovich A: **Going deeper with convolutions**. 2014:1-9.
10. Zeiler MD, Fergus R: **Visualizing and Understanding Convolutional Networks**. 2014, **8689**:818-833.
11. Srivastava N, Hinton G, Krizhevsky A, Sutskever I, Salakhutdinov R: **Dropout: a simple way to prevent neural networks from overfitting**. *Journal of Machine Learning Research* 2014, **15**(1):1929-1958.
12. Lakhani P, Sundaram B: **Deep Learning at Chest Radiography: Automated Classification of Pulmonary Tuberculosis by Using Convolutional Neural Networks**. *Radiology* 2017, **284**(2):574-582.
13. Kleesiek J, Urban G, Hubert A, Schwarz D, Maier-Hein K, Bendszus M, Biller A: **Deep MRI brain extraction: A 3D convolutional neural network for skull stripping**. *NeuroImage* 2016, **129**:460-469.
14. LeCun Y, Bengio Y, Hinton G: **Deep learning**. *Nature* 2015, **521**(7553):436-444.
15. Weiss K, Khoshgoftaar TM, Wang DD: **A survey of transfer learning**. *Journal of Big Data* 2016, **3**(1):9.
16. Pan SJ, Yang Q: **A Survey on Transfer Learning**. *IEEE Transactions on Knowledge & Data Engineering* 2010, **22**(10):1345-1359.
17. Shin HC, Roth HR, Gao M, Lu L, Xu Z, Nogues I, Yao J, Mollura D, Summers RM: **Deep Convolutional Neural Networks for Computer-Aided Detection: CNN Architectures, Dataset Characteristics and Transfer Learning**. *IEEE transactions on medical imaging* 2016, **35**(5):1285-1298.
18. Tajbakhsh N, Shin JY, Gurudu SR, Hurst RT, Kendall CB, Gotway MB, Jianming L: **Convolutional Neural Networks for Medical Image Analysis: Full Training or Fine Tuning?** *IEEE transactions on medical imaging* 2016, **35**(5):1299-1312.
19. Liu F, Jang H, Kijowski R, Bradshaw T, McMillan AB: **Deep Learning MR Imaging-based Attenuation Correction for PET/MR Imaging**. *Radiology* 2017:170700.
20. Kermany DS, Goldbaum M, Cai W, Valentim CCS, Liang H, Baxter SL, McKeown A, Yang G, Wu X, Yan F *et al*: **Identifying Medical Diagnoses and Treatable Diseases by Image-Based Deep Learning**. *Cell* 2018, **172**(5):1122-1131.e1129.
21. Asvadi NH, Afshari Mirak S, Mohammadian Bajgiran A, Khoshnoodi P, Wibulpolprasert P, Margolis D, Sisk A, Reiter RE, Raman SS: **3T multiparametric MR imaging, PIRADSv2-based detection of index prostate cancer lesions in the transition zone and the peripheral zone using whole mount histopathology as reference standard**. *Abdominal radiology (New York)* 2018, **43**(11):3117-3124.
22. Litjens G, Debats O, Barentsz J, Karssemeijer N, Huisman H: **Computer-aided detection of prostate cancer in MRI**. *IEEE transactions on medical imaging* 2014, **33**(5):1083-1092.

23. Perez L, Wang J: **The Effectiveness of Data Augmentation in Image Classification using Deep Learning**. 2017.
24. Mikołajczyk A, Grochowski M: **Data augmentation for improving deep learning in image classification problem**. In: *International Interdisciplinary Phd Workshop: 2018*; 2018: 117-122.
25. Hanley JA, McNeil BJ: **The meaning and use of the area under a receiver operating characteristic (ROC) curve**. *Radiology* 1982, **143**(1):29-36.
26. DeLong ER, DeLong DM, Clarke-Pearson DL: **Comparing the areas under two or more correlated receiver operating characteristic curves: a nonparametric approach**. *Biometrics* 1988, **44**(3):837-845.
27. Bland JM, Altman DG: **Bland JM, Altman DG. Multiple significance tests: the Bonferroni method. BMJ.310:170**. *Bmj Clinical Research* 1995, **310**(6973):170.
28. Krizhevsky A, Sutskever I, Hinton GE: **ImageNet classification with deep convolutional neural networks**. In: *International Conference on Neural Information Processing Systems: 2012*; 2012: 1097-1105.
29. Yang X, Liu C, Wang Z, Yang J, Min HL, Wang L, Cheng KT: **Co-trained convolutional neural networks for automated detection of prostate cancer in multi-parametric MRI**. *Medical image analysis* 2017, **42**:212-227.
30. Yu Y, Ji Z, Li X, Guo J, Zhang Z, Ling H, Wu F: **Transductive Zero-Shot Learning With a Self-Training Dictionary Approach**. *IEEE transactions on cybernetics* 2018.
31. Xie L, Deng Z, Xu P, Choi KS, Wang S: **Generalized Hidden-Mapping Transductive Transfer Learning for Recognition of Epileptic Electroencephalogram Signals**. *IEEE transactions on cybernetics* 2018.
32. Jiang Y, Wu D, Deng Z, Qian P, Wang J, Wang G, Chung FL, Choi KS, Wang S: **Seizure Classification From EEG Signals Using Transfer Learning, Semi-Supervised Learning and TSK Fuzzy System**. *IEEE transactions on neural systems and rehabilitation engineering : a publication of the IEEE Engineering in Medicine and Biology Society* 2017, **25**(12):2270-2284.
33. Wang X, Yang W, Weinreb J, Han J, Li Q, Kong X, Yan Y, Ke Z, Luo B, Liu T *et al*: **Searching for prostate cancer by fully automated magnetic resonance imaging classification: deep learning versus non-deep learning**. *Scientific reports* 2017, **7**(1):15415.
34. Le MH, Chen J, Wang L, Wang Z, Liu W, Cheng KT, Yang X: **Automated diagnosis of prostate cancer in multi-parametric MRI based on multimodal convolutional neural networks**. *Physics in Medicine & Biology* 2017.
35. Wang J, Wu CJ, Bao ML, Zhang J, Wang XN, Zhang YD: **Machine learning-based analysis of MR radiomics can help to improve the diagnostic performance of PI-RADS v2 in clinically relevant prostate cancer**. *European radiology* 2017, **27**(10):4082-4090.

Figures

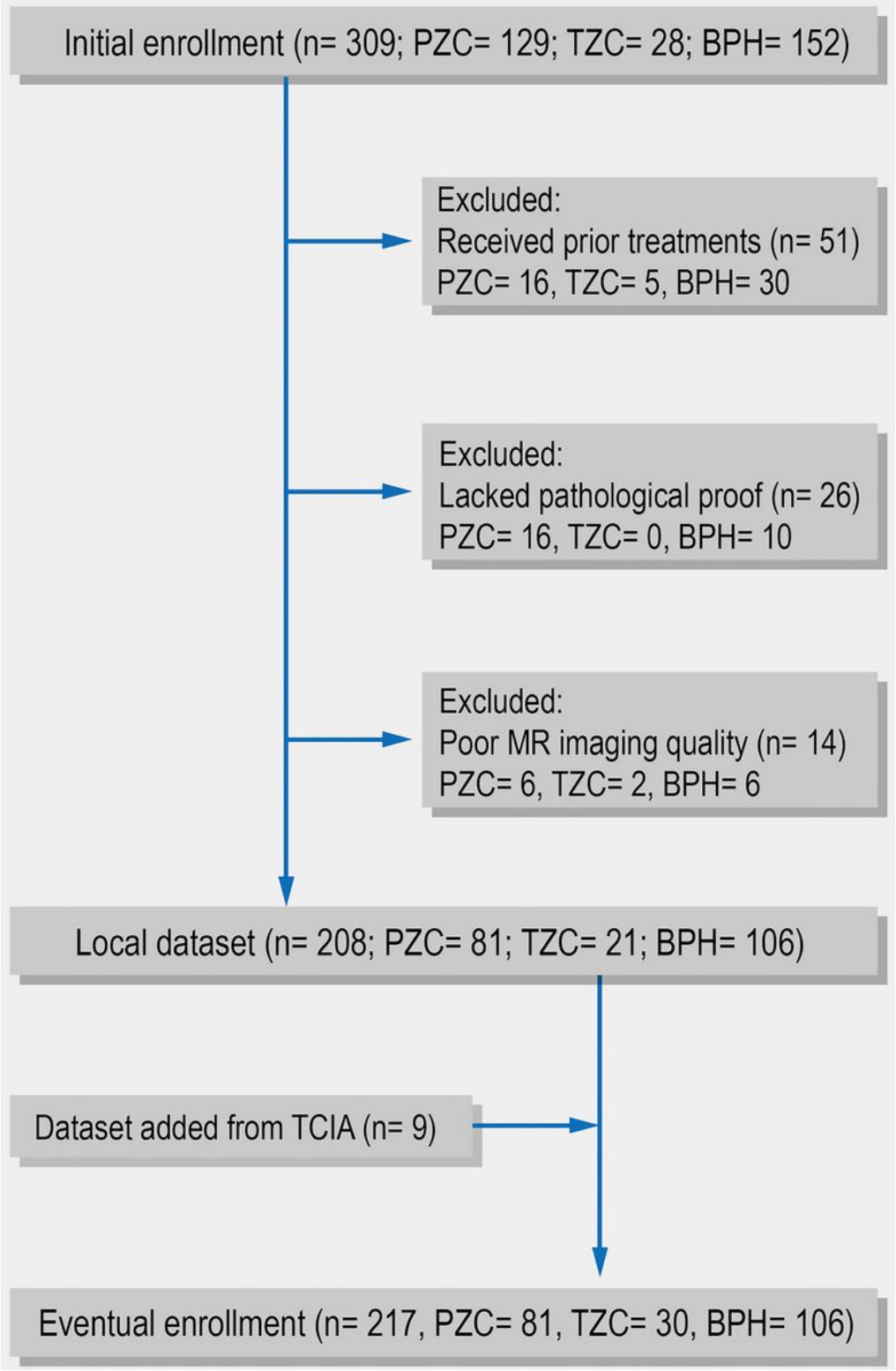

Figure 1

The patients recruiting procedure. PZC = peripheral zone cancer, TZC = transitional zone cancer, BPH = benign prostatic hyperplasia.

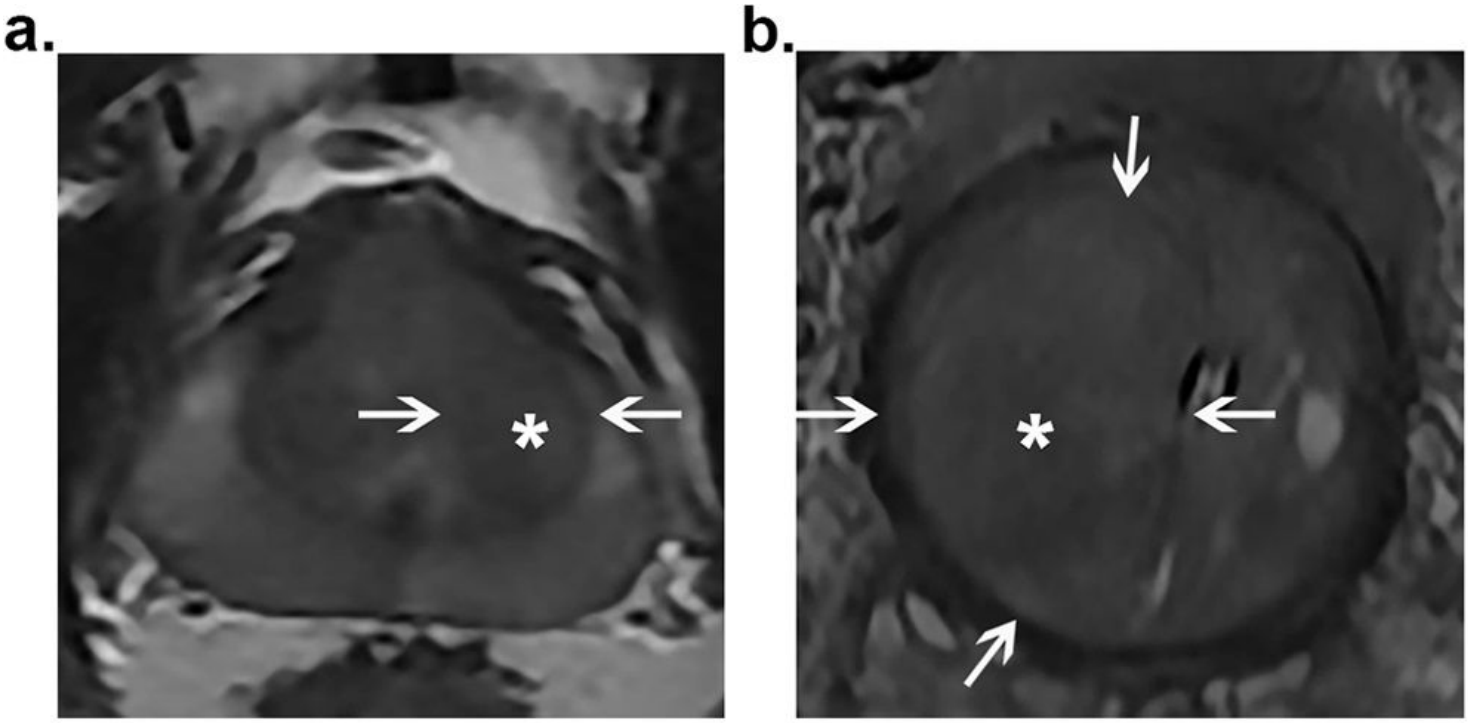

Figure 2

The confirmation process of tumor location. (A) A 60 years of man with slight urinary symptoms. This patient underwent MR imaging and was diagnosed as cancer after prostatectomy. (B) A 67 years of man with severe urinary symptoms. This patient underwent an MRI-guided biopsy and was diagnosed as benign prostatic hyperplasia.

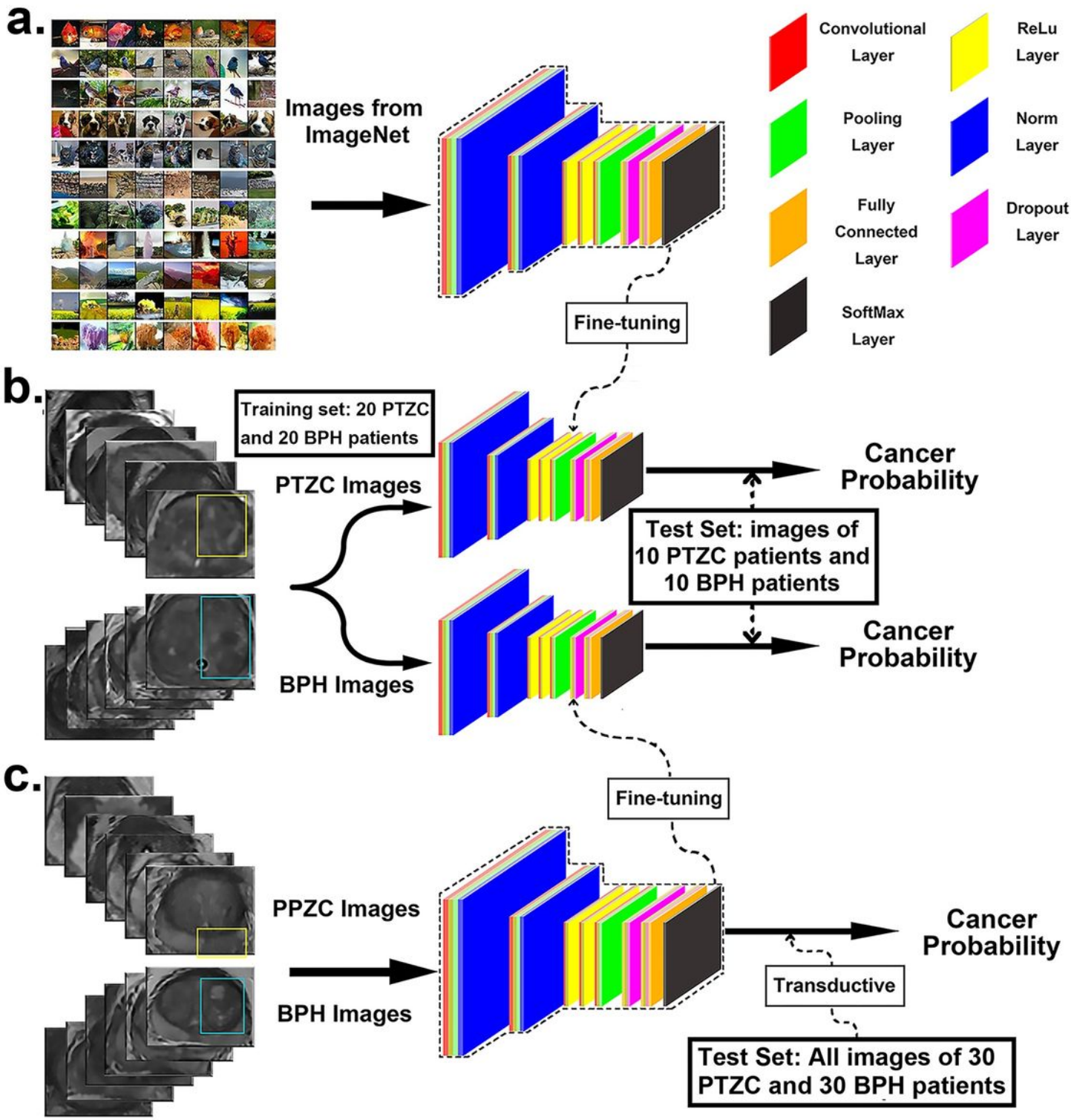

Figure 3

The procedure of TL. TL was conducted by transferring the adjustable weights from the model trained with the either data from ImageNet to our target domain (A) or disease-related domain (C). (B) Feature extraction would be conducted with “weights” of the network. After dozens or hundreds of times of training, these “weights” would be optimized. ReLu = rectified-linear activation.

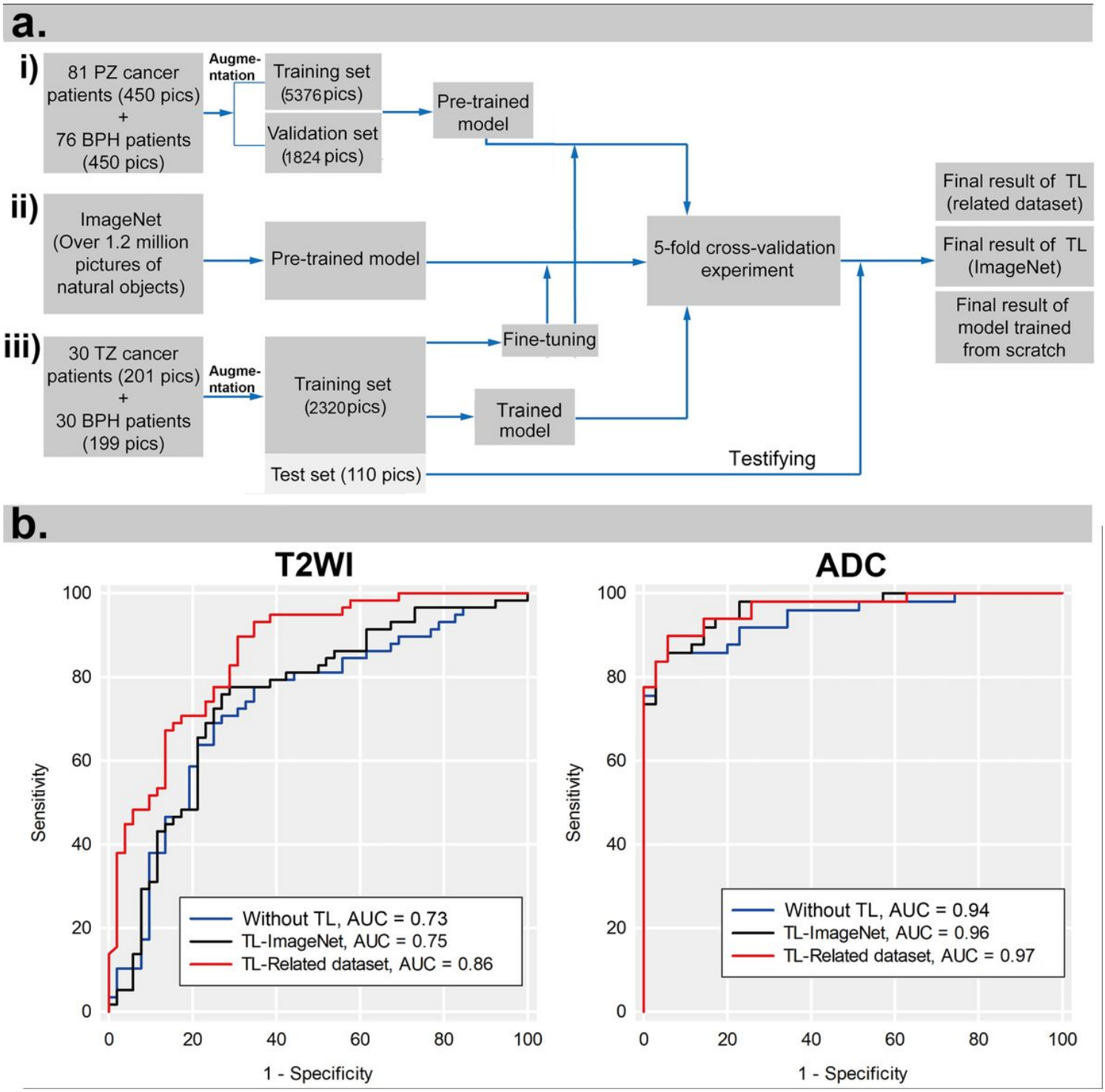

Figure 4

The experiment about the efficacy of traditional deep learning method and the TL method. (A) The flow chart of TL from disease-related data (a), TL from ImageNet (b) and without TL (c). (B) Comparison of receiver operating characteristic curves for the model trained from scratch and trained by TL. Without TL = model trained by only PTZC and BPH images. TL-ImageNet = model trained by transferring information from ImageNet. TL-Related dataset = model trained by transferring information from the disease related dataset.

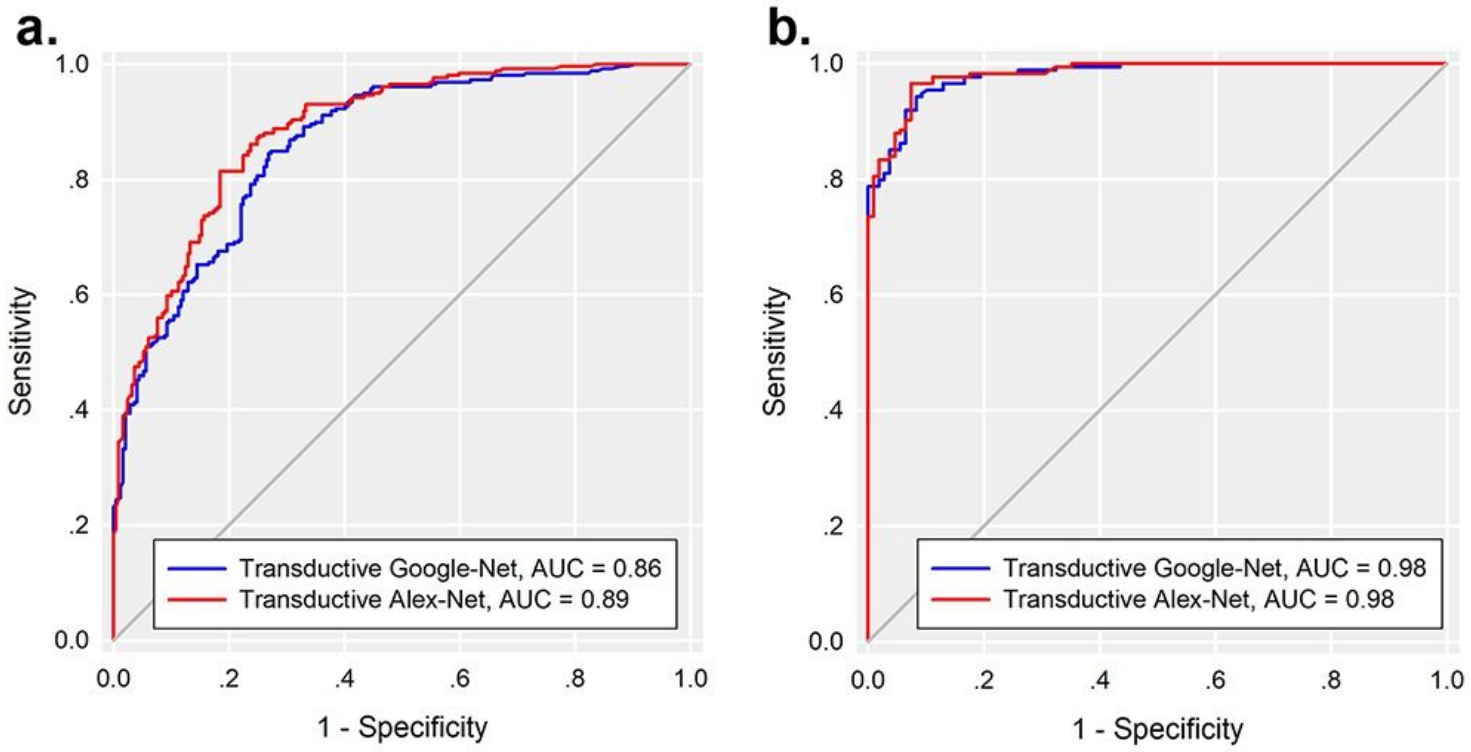

Figure 5

(A) AUCs of transductive TL Alex-Net and Google-Net models, T2WI protocol. (B) AUCs of transductive TL Alex-Net and Google-Net models, ADC maps.

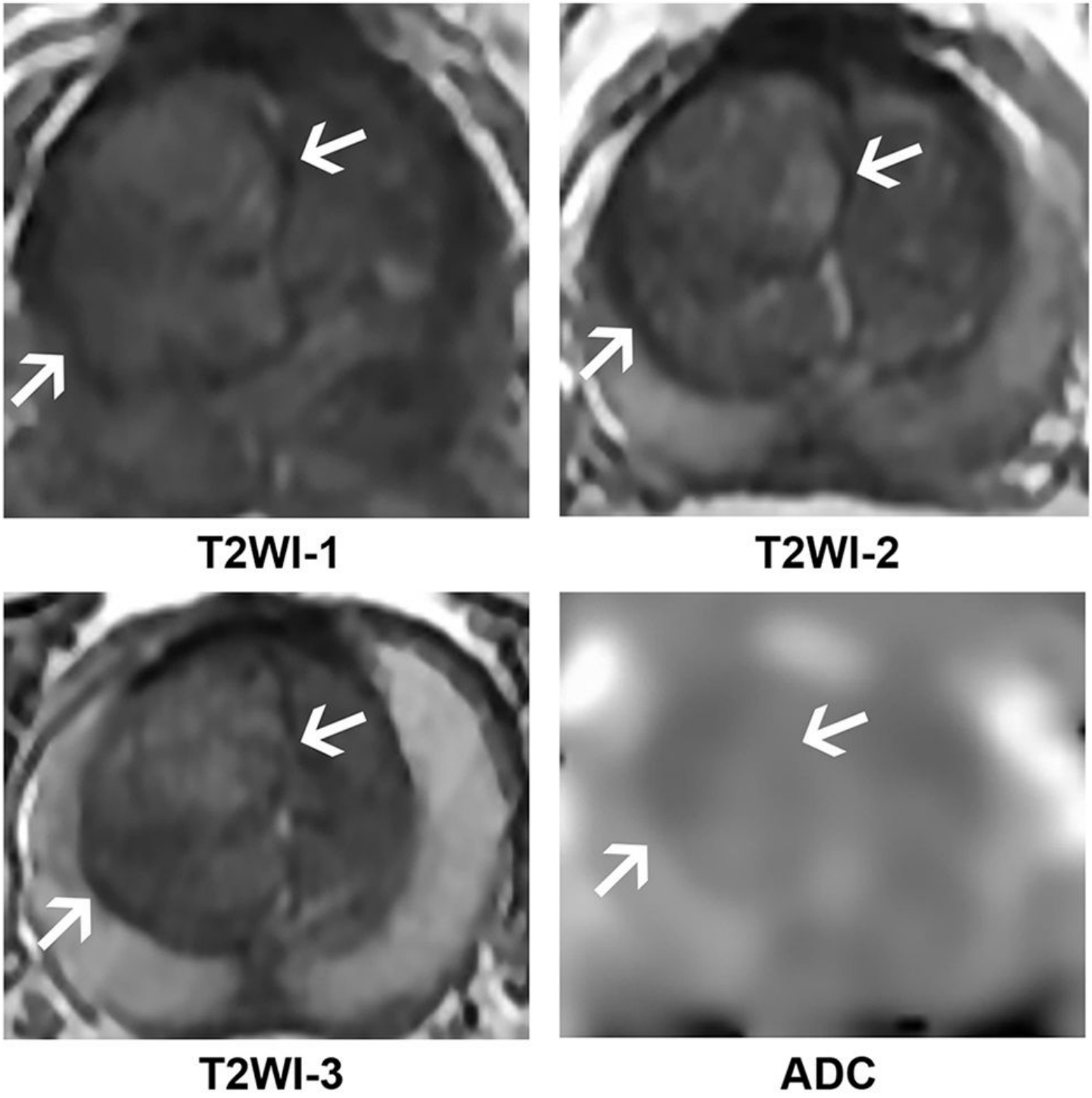

Figure 6

T2WIs and ADC map of the patient were misdiagnosed in both protocols after the ensemble procedure.

Supplementary Files

This is a list of supplementary files associated with this preprint. Click to download.

- TableS1.docx